Reconfiguration and the reduction of vortex-induced vibrations in broad leaves

6 authors, including:

Laura A Miller
University of North Carolina at Chapel Hill

87 PUBLICATIONS   **590** CITATIONS

SEE PROFILE

Christina Hamlet
Tulane University

15 PUBLICATIONS   **138** CITATIONS

SEE PROFILE

Luoding Zhu
Indiana University-Purdue University Indianap…

32 PUBLICATIONS   **853** CITATIONS

SEE PROFILE

Some of the authors of this publication are also working on these related projects:

Project   A tale of two antennules: the performance of crab odour-capture organs in air and water View project

RESEARCH ARTICLE

Reconfiguration and the reduction of vortex-induced vibrations in broad leaves

Laura A. Miller[1],*, Arvind Santhanakrishnan[2], Shannon Jones[1], Christina Hamlet[1], Keith Mertens[1] and Luoding Zhu[3]

[1]Department of Mathematics, CB 3250, University of North Carolina, Chapel Hill, NC 27599, USA [2]Department of Biomedical Engineering, Georgia Institute of Technology, 315 Ferst Drive, Atlanta, GA 30332-0363, USA and [3]Department of Mathematics, 402 N. Blackford Street, Indiana University–Purdue University Indianapolis, Indianapolis, IN 46202-3267, USA

*Author for correspondence (lam9@email.unc.edu)

SUMMARY

Flexible plants, fungi and sessile animals reconfigure in wind and water to reduce the drag acting upon them. In strong winds and flood waters, for example, leaves roll up into cone shapes that reduce drag compared with rigid objects of similar surface area. Less understood is how a leaf attached to a flexible leaf stalk will roll up stably in an unsteady flow. Previous mathematical and physical models have only considered the case of a flexible sheet attached to a rigid tether in steady flow. In this paper, the dynamics of the flow around the leaf of the wild ginger *Hexastylis arifolia* and the wild violet *Viola papilionacea* are described using particle image velocimetry. The flows around the leaves are compared with those of simplified physical and numerical models of flexible sheets attached to both rigid and flexible beams. In the actual leaf, a stable recirculation zone is formed within the wake of the reconfigured cone. In the physical model, a similar recirculation zone is observed within sheets constructed to roll up into cones with both rigid and flexible tethers. Numerical simulations and experiments show that flexible rectangular sheets that reconfigure into U-shapes, however, are less stable when attached to flexible tethers. In these cases, larger forces and oscillations due to strong vortex shedding are measured. These results suggest that the three-dimensional cone structure in addition to flexibility is significant to both the reduction of vortex-induced vibrations and the forces experienced by the leaf.

Supplementary material available online at http://jeb.biologists.org/cgi/content/full/215/15/2716/DC1

Key words: leaf design, fluid–structure interaction, immersed boundary method, mathematical model, plant biomechanics.

INTRODUCTION

Numerous investigations have shown that trees, crops and other plants often uproot or snap when they are forced by strong gusts of wind (Baker, 1995; Blackburn et al., 1988; Kerzenmacher and Gardiner, 1998). Similarly, Denny et al. (Denny et al., 1998) described how dynamic forces produced by waves are significant to the mechanical stability of the benthic organisms. Because the ability to withstand aerodynamic and hydrodynamic forces is important to the survival of many plants, a number of morphological and structural adaptations have evolved to mitigate the resulting mechanical stresses (Miller, 2005; Niklas, 1992a; Niklas, 1992b; Vincent, 1990; de Langre, 2008). The remarkable ability of plants to withstand extreme forces has generated a great deal of interest in the fields of comparative biomechanics, fluid dynamics and biologically inspired design (Alben et al., 2002; de Langre, 2008; Niklas, 1999; Speck and Burgert, 2011; Steinberg, 2002; Theckes et al., 2011). Because plant tissues generally have complex material properties, translating their design into manmade materials or mathematical models is not straightforward. Experiments with simplified physical and mathematical models have been used to elucidate the mechanical and morphological properties of plants that are fundamental to surviving extreme environments.

Plants use flexibility as one strategy to reduce the drag acting upon them while simultaneously avoiding for the most part the significant vortex-induced vibrations observed in simple flexible objects such as flags and banners. Vogel (Vogel, 1989) was the first to provide data on drag reduction due to flexibility in broad leaves. He found that single broad leaves reconfigure at high flow velocities into cone shapes that reduce flutter and drag when compared with paper cut-outs of similar shape and flexibility. At the larger scale, he also noticed that leaf clusters and leaflets tend to reconfigure into larger drag-reducing structures and speculated that similar phenomena are also true for groups of branches. If F_D is the drag acting on the leaf or bluff body, then the typical relationship between drag and velocity is given as:

$$F_D = \frac{1}{2}\rho C_D S U^2 \ , \qquad (1)$$

where ρ is the density of the fluid, U is the fluid velocity, S is the projected planar area of one side of the leaf (not taking into account reconfiguration) and C_D is the drag coefficient. Vogel (Vogel, 1989) then considered the effect of reconfiguration using the following relationship:

$$\frac{F_D}{U^2} \propto U^\beta \ , \qquad (2)$$

where β is the exponent to which the speed must be raised to be directly proportional to the drag force divided by the square of speed. The average value of β for eight tree species was –0.71. Vogel (Vogel, 2006) later found that a similar phenomenon occurs in water for herbaceous plants and proposed that this mechanism increases
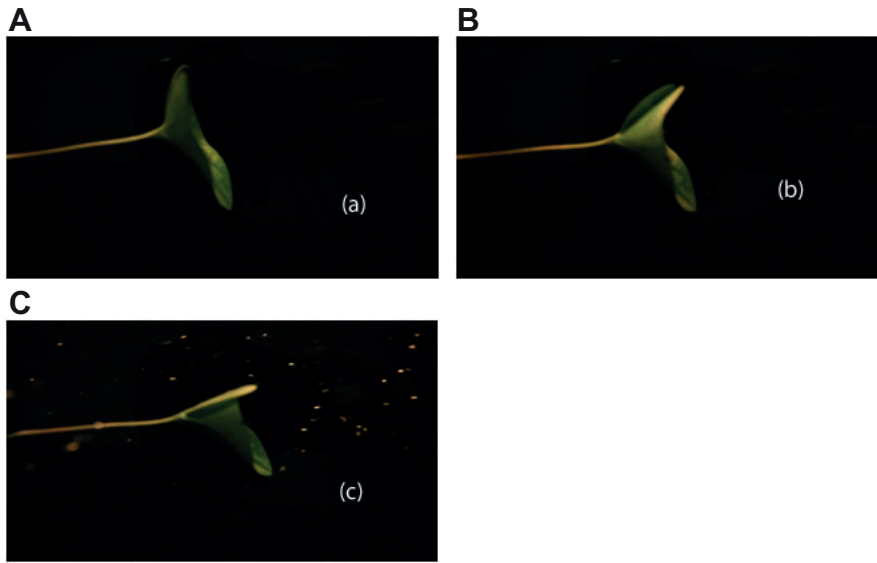
A

B

C

Fig. 1. Images of the wild ginger, *Hexastylis arifolia*, reconfiguring in flowing water as described by Vogel (Vogel, 2006). Flow speeds are (A) 0.12 m s⁻¹, (B) 0.28 m s⁻¹ and (C) 0.51 m s⁻¹.

survival rates in flash floods (see Fig. 1). Subsequent experimental studies on broad leaves and flowers also support rapid repositioning in response to strong wind as a general mechanism to reduce drag (Niklas, 1992b; Ennos, 1997; Etnier and Vogel, 2000).

A number of papers using mathematical and physical models to better understand the mechanism of drag reduction through reconfiguration have since followed this experimental work. Alben et al. (Alben et al., 2002; Alben et al., 2004) showed that simple physical and mathematical models of flexible beams immersed in steady two-dimensional flows exhibit similar drag reducing behavior. In their case, the nondimensional drag, *D*, scaled according to the equation:

$$D = C_D \eta^{4/3}, \quad \eta = \left(\frac{\rho f L^2 U^2 / 2}{E / L} \right)^{1/2}, \quad (3)$$

where *f* is the fiber thickness, *E* is the rigidity of the fiber, *L* is the fiber length and η may be thought of as the ratio of fluid kinetic energy to elastic potential energy. Zhu (Zhu, 2007; Zhu, 2008) performed similar numerical experiments of a flexible beam tethered at its center immersed in a two-dimensional (2-D) steady flow using the immersed boundary method. As Reynolds number (*Re*) was increased from 10 to 800, Zhu found that the exponents of the power laws decreased monotonically from approximately 2 towards 4/3. Schouveiler and Boudaoud (Schouveiler and Boudaoud, 2006) showed experimentally that flexible sheets with rigid tethers can roll up into cone shapes in steady flow, also reducing the drag acting upon them. Gosselin et al. (Gosselin et al., 2010) considered flexible plates with rigid tethers in a steady wind tunnel. For both a single plate and a set of plates arranged in a rosette pattern, the experimental results were well explained by the theory introduced by Alben et al. (Alben et al., 2002).

The previous work with physical and mathematical models has focused on reconfiguration in steady flow with rigid attachments, but flexible bodies attached to moving tethers in unsteady flows experience strong oscillations and higher peak drag. Vogel (Vogel, 1989) compared the drag generated by flexible sheets and leaves of similar elastic properties and found that the forces generated by the flexible sheets were at least three times higher. He also noted that flutter was substantially reduced in broad leaves relative to paper cut-outs. Flutter occurs when a positive feedback exists between a structure's natural vibration and aerodynamic forces and is included in a larger set of phenomenon defined as vortex-induced vibrations. Because the results of such vibrations can be devastating, a large amount of research in structural dynamics has focused on improving aeroelastic behavior by modifying the cross-sectional shapes and material properties of structures to avoid self-excitation (Tomita et al., 1988; Luongo and Piccardo, 1998; Wilson, 1984).

Although it is now clear that flexible plants can reduce drag through reconfiguration, it is not at all obvious how leaves and branches minimize the effects of vortex-induced oscillations. Niklas and Brüchert et al. (Niklas, 1992a; Brüchert et al., 2003) suggest that structural damping can play an important role, and Miller (Miller, 2005) showed that stiffness nonlinearities can reduce the amplitudes of these destructive oscillations. The effect of shape and other material properties on this complex fluid–structure interaction problem, however, remains relatively unexplored. Advanced engineering structures similarly include material properties and shapes that help reduce vortex-induced vibration, and comparisons between natural and manmade structures could enhance our understanding of natural adaptions while improving some aspects of engineering design.

In this study, 2-D numerical simulations using the immersed boundary method were used to solve the fully coupled fluid–structure interaction problem of a flexible beam (leaf) attached to a flexible tether (leaf stalk) in steady flow. The goal of these numerical simulations was to determine whether the addition of a flexible tether to the simple 2-D reconfiguration model proposed by Alben et al. (Alben et al., 2002) and simulated by Zhu (Zhu, 2007) can lead to vortex-induced vibrations and large forces that do not characterize actual leaves. Specifically, the dimensionless drag over time was calculated to determine whether the addition of a flexible tether increased the drag acting upon the beam relative to similar beams with rigid attachments. Significant differences in peak forces would indicate some limitations of the simple 2-D reconfiguration model and motivate further study of vibration-reducing mechanisms in leaves.

To explore the role of the three-dimensional (3-D) reconfiguration shape on the reduction of vortex-induced vibrations, drag was measured over a range of speeds for physical models of sheets attached to flexible beams that reconfigure into cones and U-shapes. Dynamic forces were compared with those reported for broad leaves

in air and water. The wakes generated behind the physical models and the leaves of the wild ginger *Hexastylis arifolia* and the wild violet *Viola papilionacea* were quantified using 2-D planar particle image velocimetry (PIV).

MATERIALS AND METHODS
Model equations and dimensionless parameters

The full Navier–Stokes equations were used to describe the motion of the fluid. The 2-D equations can be rewritten in dimensionless form as follows:

$$\frac{\partial \mathbf{u}'}{\partial t} + \mathbf{u}' \cdot \nabla' \mathbf{u}' = -\nabla' p' + \frac{1}{Re} \nabla'^2 \mathbf{u}' + \mathbf{f}'$$

$$\nabla' \cdot \mathbf{u}' = 0 . \tag{4}$$

$$Re = \frac{\mu L U}{\rho} . \tag{5}$$

$$\mathbf{u}' = \frac{\mathbf{u}}{U} \qquad t' = \frac{tU}{L}$$

$$p' = \frac{p}{\rho U^2} \qquad \mathbf{x}' = \frac{\mathbf{x}}{L} \quad , \tag{6}$$

$$\mathbf{f}' = \frac{\rho U^2 \mathbf{f}}{L} \qquad \nabla' = L\nabla$$

where $\mathbf{u}$ is the fluid velocity, p is the pressure, $\mathbf{f}$ is the force per unit area applied to the fluid by the immersed boundary, ρ is the density of the fluid, μ is the dynamic viscosity of the fluid, t is dimensional time and $\mathbf{x}$ is the position in Cartesian coordinates. Note that ∇ denotes the gradiant. The dimensionless variables are $\mathbf{u}'$, $\mathbf{x}'$, p', t' and $\mathbf{f}'$, which represent the dimensionless velocity, position, pressure, time and force per unit area, respectively. L is a characteristic length (such as the length of the leaf) and U is a characteristic velocity (such as the maximum free stream velocity) used in the nondimensionalization. Re is then given by Eqn 5 and represents the order of magnitude of the ratio of inertial and viscous forces in the fluid.

The dimensionless equation describing a one-dimensional elastic structure in a fluid can be written as follows (Alben, 2008; Alben, 2009):

$$m' \frac{\partial^2}{\partial t'^2} \mathbf{X}(s',t') = \frac{\partial}{\partial s'}(T\hat{s}) - k'_{bend} \frac{\partial^2}{\partial s'^2}(\overline{\kappa}\hat{n}) + \mathbf{F}' , \tag{7}$$

where m' is the dimensionless mass, s' is the dimensionless arc length, T is the tension, k'_{bend} is the dimensionless bending stiffness, $\mathbf{F}'$ is the dimensionless force per unit length acting on the structure, $\overline{\kappa}$ is the curvature, $\hat{n}$ is the unit vector pointing normal to the boundary and $\hat{s}$ is the unit vector tangent to the boundary. The dimensionless mass and bending stiffness of the boundary may then be written as:

$$k'_{bend} = \frac{EI}{\rho U^2 L^3} , \tag{8}$$

$$m' = \frac{\rho_s}{\rho L} , \tag{9}$$

where ρ_s is the mass per unit length of the boundary and EI is the dimensional flexural stiffness. The dimensionless bending stiffness, k'_{bend}, may also be considered as the dimensionless flexural stiffness.

Numerical method

In this paper, the 2-D immersed boundary method is used to simulate a flexible fiber (equivalent to a sheet in the 3-D fluid)
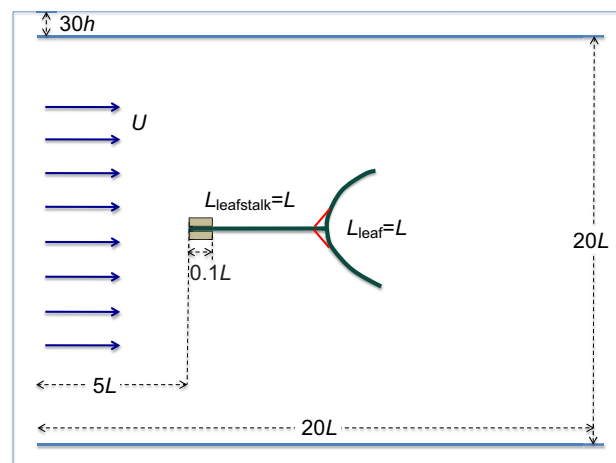

Fig. 2. Numerical setup of the immersed boundary simulations. Flow is driven past a flexible leaf modeled here in one dimension as a beam (the two-dimensional interpretation in three-dimensional flow is a sheet) with a length set to L_{leaf}. The leaf is then attached to a flexible leafstalk of length $L_{leafstalk}$ modeled as a beam that is fixed at its base. The attachment of the leaf to the leafstalk is made using a pair of springs that resists deflections from 90 deg of the leaf relative to the leafstalk. h, height.

attached to a flexible beam immersed in a viscous, incompressible fluid (Fig. 2). The immersed boundary method has been used successfully to model a variety of problems in fluid dynamics where the interactions between an incompressible viscous fluid and a deformable elastic boundary are significant. Some examples of biological problems that have been studied with the immersed boundary method include lamprey swimming (Tytell et al., 2010), jellyfish feeding (Hamlet et al., 2011), flow-through heart valves (Griffith et al., 2009) and ciliary-driven flows (Grünbaum et al., 1998).

In the immersed boundary framework, the Navier–Stokes equations (Eqn 4) are solved on a fixed Cartesian grid. The elasticity equation for the boundary (Eqn 7) is solved on a moving Lagrangian grid. The fluid equations are coupled to the boundary equations through the following fluid–structure interaction equations:

$$\mathbf{f}'(\mathbf{x}',t') = \int \mathbf{F}'(\mathbf{X}'(s',t'),t')\delta(\mathbf{x}' - \mathbf{X}'(s',t'))\mathrm{d}s' , \tag{10}$$

$$\frac{\partial \mathbf{X}'(s',t')}{\partial t'} = \mathbf{U}'(\mathbf{X}'(s',t')) = \int \mathbf{u}'(\mathbf{x}',t')\delta(\mathbf{x}' - \mathbf{X}'(s',t'))\mathrm{d}\mathbf{x}' , \tag{11}$$

where $\mathbf{F}'(s',t')$ is the dimensionless force per unit length acting on the fluid, $\mathbf{X}'(s',t')$ gives the dimensionless Cartesian coordinates of the boundary and $\mathbf{U}'(s',t')$ is the dimensionless local fluid velocity at the boundary point s'. Eqn 10 communicates the force exerted by the boundary on the fluid grid using a smoothed 2-D Dirac delta function $\delta(\mathbf{x}')$. Once the Navier–Stokes equations have updated the fluid information for the time step, Eqn 11 is used to interpolate the local fluid velocity at each boundary point and move the boundary at the estimated velocity. This enforces the no-slip condition associated for a viscous fluid.

The exact numerical algorithm used in this paper is described in detail in Peskin and McQueen (Peskin and McQueen, 1996) with the exception of the discretization of the δ-function. The choice of δ-function used here is detailed in Peskin and Printz (Peskin and Printz, 1993) and is given by the following equations:

$$\delta_{\Delta x'} = \Delta x'^{-2} \phi\left(\frac{x'}{\Delta x'}\right) \phi\left(\frac{y'}{\Delta x'}\right), \qquad (12)$$

$$\phi(r) = \begin{cases} \frac{1}{4}\left(1 + \cos\left(\frac{\pi r}{2}\right)\right), & |r| \le 2 \\ 0, \text{otherwise} \end{cases}, \qquad (13)$$

where $\Delta x'$ is the spatial step size in both the x'- and y'-directions, and $\delta_{\Delta x'}$ denotes the discretized version of the δ-function.

Numerical setup

In the following simulations, a computational channel was used with dimensions $20L \times 20L$. To avoid the placement of target points directly on the boundary and reflection of forces across the periodic domain, this channel was placed within a slightly larger periodic domain, of size $(20L+30h) \times (20L+30h)$, where $h = \Delta x' = \Delta y'$ is the mesh width of the fluid grid and $L = 0.0333h$. The two edges of the computational channel oriented parallel to the flow were made of immersed boundary points that were linked by stiff linear springs to stationary target points with dimensionless stiffness $k'_{\text{targ}} = 10$. The Navier–Stokes equations were solved on a 630×630 Cartesian grid, and the fiber and beam attachments were each discretized on a Lagrangian array of 60 points.

Parabolic flow with maximum velocity U'_{max} was driven within the channel and upstream of the model leaf by applying an external force, $\mathbf{f}'_{\text{ext}}$, to the fluid proportional to the difference between the desired fluid velocity and the actual fluid velocity. Parabolic flow was applied because this is the steady-state profile for flow through a channel at this Re. This force was applied to a strip of width $L/6$ upstream of the base of the attachment using the following equations:

$$\mathbf{f}'_{\text{ext}}(i,j) = \begin{cases} -k_{\text{ext}}\left(\mathbf{u}'(i,j) - \mathbf{u}'_{\text{targ}}(i,j)\right), \\ 0 \le jh \le 20L, 10 \le i \le 15 \\ 0, \text{otherwise} \end{cases}, \qquad (14)$$

$$\mathbf{u}'_{\text{targ}}(i,j) = \begin{bmatrix} U'_{\text{max}}\left(1 - \left(\frac{0.5 - jh}{10L}\right)^2\right) \\ 0 \end{bmatrix}. \qquad (15)$$

Note that the maximum velocity occurs in the middle of the channel, and the indices of j are equal to $-1, -2$, etc. for regions of the domain below the immersed floor. The difference between the actual and desired velocities was controlled with a 'stiffness' parameter, $k'_{\text{ext}} = 10$, such that the difference between the two velocities was always less than 0.1%.
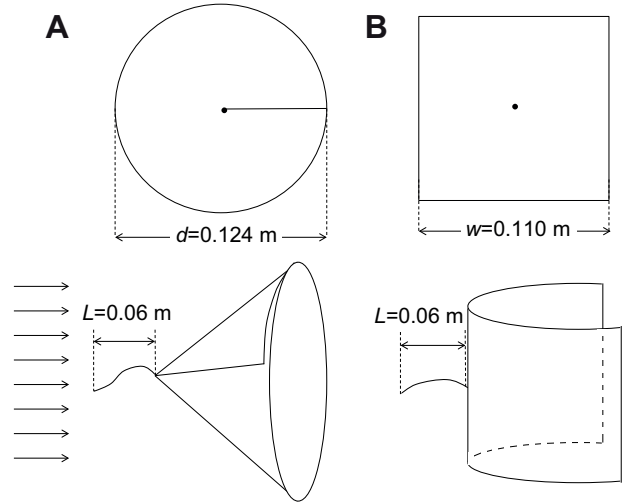

Fig. 3. Diagram of the physical models used for force measurements and flow visualization with particle image velocimetry (PIV). (A) The cone shape model was constructed by cutting a circle out of transparency paper and cutting a slit from the center to the edge. The reconfigured shape of the model is shown below. (B) The U-shape model was constructed by cutting a square out of transparency paper. The reconfigured shape of the model is shown below.

Dimensionless lift and drag were calculated as functions of time by summing the forces at each immersed boundary point at each time step and taking the opposite sign of that value. In this paper, the dimensionless lift force, F'_L, is defined as the force acting perpendicular to the direction of flow, and the dimensionless drag, F'_D, is defined as the force acting parallel to the direction of flow.

Leaves and physical models

The wild ginger *Hexastylis arifolia* and the wild violet *Viola papilionacea* were collected from the banks of Jordan Lake in Alamance County, NC, and the Eno River in Orange County, NC, respectively. Both were potted in moist commercial soil for transport back to the laboratory. The specimens were kept indoors with a grow light and were tested within 1 week of collection. Leftover specimens remained healthy in the laboratory for months after the experiments and appeared to show no damage from collection. Branches from the tulip tree *Liriodendron tulipifera* were collected in August in Orange County, NC, and used within 2 h. Leaves were removed from the branches immediately before placing them in the wind tunnel for drag measurements. Artificial models were constructed from clear acetate 5 µm transparency film (Precision Image, Austin, TX, USA). The models were either squares or circles (Fig. 3). The circular models were cut with a slit from the edge to the center to allow for

Table 1. Length (L), width (W), thickness (T), elastic modulus (E) and dimensionless bending stiffness (k_{bend}) for ginger and model leaves

Sample	L (m)	W (m)	T (m)	E (N m^{-2})	k_{bend}
Hexastylis (PIV)	$(8.81\pm1.74)\times10^{-2}$	$(5.87\pm1.86)\times10^{-2}$	1.5×10^{-3}	$(2.6\pm2.5)\times10^{7}$	2.4×10^{-3} (U=0.53 m s^{-1})
Cone (PIV)	Diameter=8.73×10^{-2}	n/a	1.27×10^{-4}	4.6×10^{9}	4.2×10^{-3} (U=0.53 m s^{-1})
U-shape (PIV)	9.05×10^{-2}	9.05×10^{-2}	1.27×10^{-4}	4.6×10^{9}	3.8×10^{-3} (U=0.53 m s^{-1})
Cone (force in water)	Diameter=1.24×10^{-1}	n/a	1.27×10^{-4}	4.6×10^{9}	1.5×10^{-3} (U=0.53 m s^{-1})
U-shape (force in water)	1.10×10^{-1}	1.10×10^{-1}	1.27×10^{-4}	4.6×10^{9}	2.7×10^{-3} (U=0.53 m s^{-1})
Cone (force in air)	Diameter=1.24×10^{-1}	n/a	1.27×10^{-4}	4.6×10^{9}	5.3×10^{-3} (U=8 m s^{-1})
U-shape (force in air)	1.10×10^{-1}	1.10×10^{-1}	1.27×10^{-4}	4.6×10^{9}	9.7×10^{-3} (U=8 m s^{-1})

PIV, particle image velocimetry.
The cone and U-shape models were made from clear acetate 5 µm transparency film.

Table 2. Dimensions of ginger leafstalks and model attachment beams

Sample	L (m)	R (m)	E (N m^{-2})	k_{bend}
Leafstalk	$(7.94\pm2.95)\times10^{-2}$	$(9.90\pm1.75)\times10^{-4}$	$(2.14\pm1.51)\times10^{6}$	2.0×10^{4}
Rigid rod	8.75×10^{-2}	4.76×10^{-3}	Rigid	Rigid
Flexible beam	6.83×10^{-2}	7.50×10^{-4}	$(9.62\pm7.63)\times10^{6}$	3.0×10^{4}

L, length of beam; R, radius of specimens; E, Young's modulus; k_{bend}, dimensionless bending stiffness.

reconfiguration into a cone under flow. All models were attached at their centers to either a rigid rod or a flexible plastic beam. This allowed the square models to reconfigure into a U-shape and the circular models to reconfigure into cones. The dimensional and dimensionless lengths and bending stiffnesses of the leaves, models and attachments are summarized in Tables 1 and 2.

Flow tank and wind tunnel
For aquatic measurements, drag measurements and flow measurements using PIV were performed on single leaves and models clamped at the proximal ends of their leafstalks (or beam attachments) in a drafting fork as described by Vogel (Vogel, 2006). The flow tank contained a 0.350×0.325 m working cross-section and was similar to that described by Vogel and LaBarbera (Vogel and LaBarbera, 1978). Drag measurements were taken using flow-straightening collimators placed upstream and downstream of the working section. For the PIV measurements, the collimators were removed in a manner similar to that used in Vogel's experiments on *Hexastylis* (Vogel, 2006). Average flow velocities were measured using a Vernier Software & Technology flow rate sensor (FLO-BTA, Beaverton, OR, USA). The flow velocity used for PIV was set to $0.53\,\mathrm{m\,s^{-1}}$ unless otherwise noted. The flow velocities for the force measurements were varied from 0.3 to $1\,\mathrm{m\,s^{-1}}$.

For aerial force measurements, the models were mounted in the working section of an open circuit wind tunnel (Tucker and Parrott, 1970). Wind velocities were measured using a Fisher Scientific Traceable Digital Anemometer (Hampton, NH, USA). Wind speeds were increased in $0.5\,\mathrm{m\,s^{-1}}$ increments and were varied from 3 to $11\,\mathrm{m\,s^{-1}}$. Models were attached to the base of an aluminum beam using a flexible beam of 6 cm length (see details below).

Particle image velocimetry
Flow velocity measurements were made using 2-D planar instantaneous and time-averaged PIV. The laser sheet for the PIV measurements was generated from a 50 mJ double-pulsed Nd:YAG

laser (Continuum, Santa Clara, CA, USA), which emitted light at a wavelength of 532 nm with a maximum repetition rate of 15 Hz. The laser beam was converted into a planar sheet approximately 3 mm thick using a set of focusing optics. The laser sheet was located in the *x–y* plane upstream of the working section. A mirror was used to reflect the laser sheet down onto the leaf (Fig. 4). The time

Fig. 5. Vorticity plots for varying dimensionless bending stiffness, k_{bend}. Warm colors show regions of positive vorticity and cool colors show regions of negative vorticity. The model leaf and leafstalk are shown in magenta. (A) The bending stiffness of the leaf and leafstalk was set to $k_{bend}=10^{-2}$. Some reconfiguration and oscillations of the model occur because of vortex separation in the wake. (B) The bending stiffness of the leaf was set to $k_{bend}=10^{-2}$, but the tether was rigid. Reduced oscillations are observed. (C) The bending stiffness of the leaf and attachment were set to $k_{bend}=10^{-1}$, and a strong wake of alternating vortices is present. (D) The bending stiffness of the leaf and attachment was set to $k_{bend}=10^{-3}$. For this set of parameters, oscillations and drag are reduced due to reconfiguration.
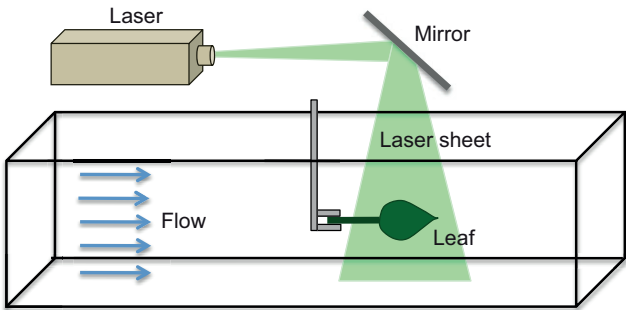

Fig. 4. Schematic of the PIV apparatus and flow tank. Water is driven through the working section of a flow tank with the collimators removed to create unsteady flow as described in Vogel (Vogel, 2006). A leaf or leaf model is then lowered into the middle of the working section of the tank with the base of its leafstalk clamped to a fixed structure. A mirror is used to reflect a laser sheet into the tank to illuminate the flow around the leaf.
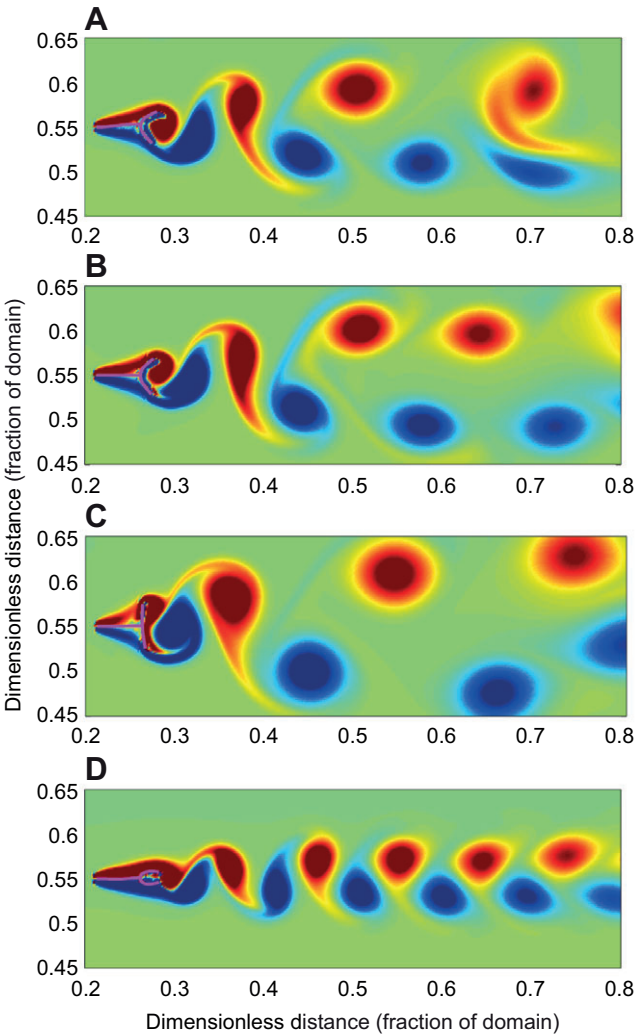
interval of separation between two image pairs was varied from 125–150 µs. A 14 bit CCD camera (Imager Intense, LaVision, Ypsilanti, MI, USA) with a 1376×1040 pixel array was used to capture images. The spatial resolution was approximately 0.05 mm pixel^{-1}. Uniform seeding was accomplished using 10 µm hollow glass spheres that were inserted in the flow tank and mixed to achieve a near-homogeneous distribution prior to each experiment. Volume fractions were such that approximately 40–50 particles were visible within each 64×64 pixel window. In typical experiments there was a maximum particle displacement of 0.8 mm (or 14 pixels) within the correlation window, which corresponds to 25% displacement in a 64×64 pixel window.

For the actual leaves, the PIV analysis was performed beyond the point where the leaf surface was reconfigured and remained static during the entire time of acquisition. Hence, no masking of the leaf surface was performed. The physical models were transparent so that the masking of these surfaces was not necessary. Image pairs were analyzed using a single pass cross-correlation algorithm in Davis 7.0 (LaVision) using interrogation windows of size 64×64 pixels with 50% overlap. No pre-processing of the raw data was performed prior to this step. For each PIV set of time averaged data, 204 images were recorded for processing, resulting in a total of 102 velocity vector fields from which to generate mean flow field and statistics. No smoothing algorithms or other post-processing techniques were employed on the data.

Drag measurements

Drag was measured using a method similar to that described in Vogel (Vogel, 1989). Strain gauges (120 ohm) were affixed to opposite sides of an aluminum beam. The beam was arranged as a cantilever beam that was 1.27 mm thick, 14 mm wide and 135 mm long. The natural frequency of the beam was approximately 54 Hz in air and 30 Hz in water. The strain gauges made up two arms of an ordinary DC Wheatstone bridge. The imbalance of the bridge fed into a computer through a National Instruments DAQ (cDAQ-9172, Austin, TX, USA) and recorded at a sampling rate of 1000 Hz using MATLAB software (The MathWorks, Natick, MA, USA). The signal was then processed in MATLAB using a Butterworth low-pass filter (120 Hz cutoff frequency) and 60 Hz band-stop filter. The cantilever beam was gravimetrically calibrated while clamped horizontally by hanging weights from the attachment site.

RESULTS AND DISCUSSION
Numerical simulations

To examine the effect of varying stiffness on reconfiguration shapes and forces generated by model leaves attached to flexible beams in steady flow, numerical simulations were performed at $Re=235$ for $k'_{bend}=2\times10^{-1}$, 2×10^{-2}, 10^{-2} and 10^{-3}. Vorticity snapshots taken at $t'=120$ are shown in Fig. 5. Warm colors represent regions of positive vorticity and cool colors show regions of negative vorticity. The model leaf and leafstalk are shown in magenta. When the leaf and leafstalk were set to $k'_{bend}=10^{-2}$, the leaf reconfigured into a U-shape and some oscillations occurred because of vortex separation in the wake of the model (Fig. 5A, see supplementary material Movie 1). When the bending stiffness of the leaf was kept at $k'_{bend}=10^{-2}$ and the tether was made rigid, the leaf again reconfigured into a U-shape but reduced oscillations were observed (Fig. 5B, see supplementary material Movie 2). The bending stiffness of the leaf and attachment were then made stiffer and set to $k'_{bend}=2\times10^{-1}$ and a strong wake of alternating vortices was present (Fig. 5C, see supplementary material Movie 3). Finally, the bending stiffness of the leaf and attachment were made rather flexible with $k'_{bend}=10^{-3}$. For this set of parameters, oscillations and drag were reduced because of substantial reconfiguration and reduced frontal area of the leaf (Fig. 5D).

Dimensionless drag and lift are shown as functions of dimensionless time, t', in Fig. 6. In general, average forces decrease as the bending stiffness decreases. The initial increase in the drag ($0<t'<5$) was due to the acceleration of the fluid. For $k'_{bend}=2\times10^{-1}$, 2×10^{-2} and 10^{-2} there was an initial decrease in drag ($5<t'<20$) followed by an increase in both the magnitude and amplitude of oscillations ($t'>20$). An inspection of the corresponding movie (see supplementary material Movies 1–3) showed that this increase corresponded to the onset of large vortex. The amplitude of the oscillations of the lift forces also increased as the system settled into a state of large vortex separation coupled to the oscillation of the leaf for $t'>20$. Taking into account both components of the force, the total peak forces on the leaf are 1.5 to three times higher after the onset of large vortex-induced oscillations.

Fig. 7 shows the average dimensionless forces calculated before the onset of vortex shedding ($10<t'<20$) and after the onset of vortex shedding ($t'>40$). The average magnitude of the dimensionless force was calculated as $F'=\sqrt{F_D'^2+F_D'^2}$. For the purpose of quantifying the
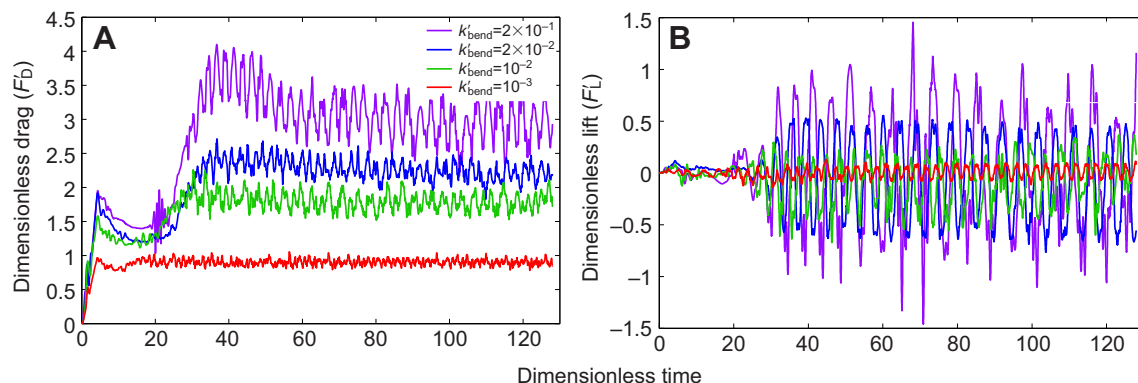

Fig. 6. Dimensionless drag and lift as functions of dimensionless time, t'. In these numerical simulations, flow is driven past a flexible leaf attached to a flexible leafstalk at $Re=235$ for dimensionless bending stiffnesses set to $k'_{bend}=2\times10^{-1}$, 2×10^{-2}, 10^{-2} and 10^{-3}. In general, average forces decrease as the bending stiffness decreases. (A) The initial increase in the drag ($0<t'<5$) is due to the acceleration of the fluid. There is an initial decrease ($5<t'<20$) followed by an increase in both the magnitude and degree of oscillations ($t'>20$). An inspection of the movies (see supplementary material Movies 1–3) shows that this increase corresponds to the onset of large vortex separation coupled to the oscillations of the leaf. (B) The magnitude of the lift forces perpendicular to the direction of flow also increase as the system settles into a state of large vortex separation coupled to the oscillation of the leaf for $t'>20$.
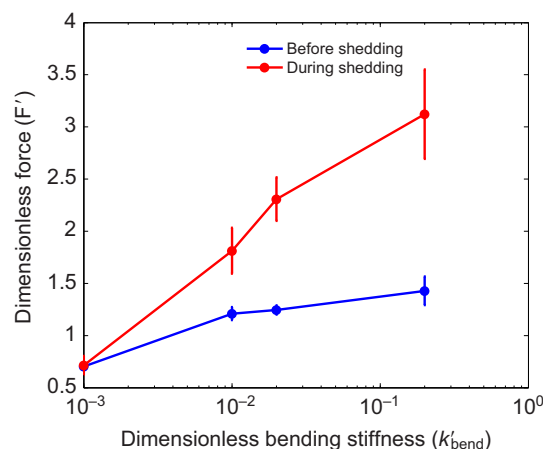
Fig. 7. Average force coefficients *versus* the dimensionless bending coefficient, k_{bend}, calculated before the onset of vortex shedding for $10 < t' < 20$ and after the onset of vortex shedding for $t' > 40$. For the purpose of quantifying the variations in peaks, the vertical bars show the standard deviations in the force measurements. Note that the average force acting on the model leaf during vortex shedding is more than twice as much as that before vortex shedding for the stiffest model. The average force measured during shedding approaches the force measured before shedding for the most flexible models.

Fig. 8. Vorticity plots for increasing free-stream velocities set to $U'_{max}=\frac{1}{2}$, 1, 2 and 4 (top to bottom) with $k'_{bend}=10^{-2}$. Warm colors show regions of positive vorticity and cool colors show regions of negative vorticity. The amount of reconfiguration increases as the velocity increases. The width of the vortex wake decreases as the velocity increases, which is partially responsible for the reduction in drag. In the last image, the tips of the model leaf have adhered together because of effects, stabilizing the leaf (see supplementary material Movie 5).

variations in peaks, the vertical bars on the graph show the standard deviation in the force measurements. This analysis was performed to quantify the effect of vortex-induced vibrations on the fluid dynamic forces acting on the models. Average forces taken before vortex shedding are comparable to those reported by Zhu (Zhu, 2007; Zhu, 2008). The average force generated during vortex shedding is more than twice as much as that generated before vortex shedding for the stiffest model ($k'_{bend}=2\times10^{-1}$). This difference decreases as the flexibility increases.

To consider the effect of increased velocity and frequency of vortex shedding, numerical simulations were performed for $U'_{max}=\frac{1}{2}$, 1, 2 and 4 and with $k'_{bend}=10^{-2}$. Here k'_{bend} is determined by normalizing the bending stiffness with respect to a fixed $U=1$. Vorticity snapshots taken at $t'=120$ are shown in Fig. 8. Warm colors represent regions of positive vorticity and cool colors show regions of negative vorticity. The amount of reconfiguration increased as the velocity increased (see supplementary material Movies 4, 5). The width of the vortex wake decreased as the velocity increased, which correlates to the reduction in dimensionless drag. Fig. 8D and supplementary material Movie 5 show an interesting result that is due to numerical effects. At $t'\approx80$, the tips of the leaf adhered to each other, effectively locking the model into a streamlined shape. As a result, both oscillations and drag are reduced for $t'>80$. This numerical error was due to under-resolving the flow near two ends of the immersed boundary, but it does illustrate how a body stuck in a streamlined position potentially experiences lower drag.

Dimensionless lift and drag are plotted as functions of dimensionless time for the above four velocities with $k'_{bend}=10^{-2}$ in Fig. 9. For free-stream velocities set to $U_{max}=\frac{1}{2}$, 1 and 2, the magnitudes of the dimensionless lift and drag decreased as the velocity increased because of the reconfiguration of the model leaf. Force coefficients then increased as the velocity increased to 4 because the interaction of the fluid and structure created larger oscillations of the leaf. Around $t'=80$, the tips of the model leaf adhered as a result of numerical error, and the dimensionless drag and amplitude of the oscillations decreased.
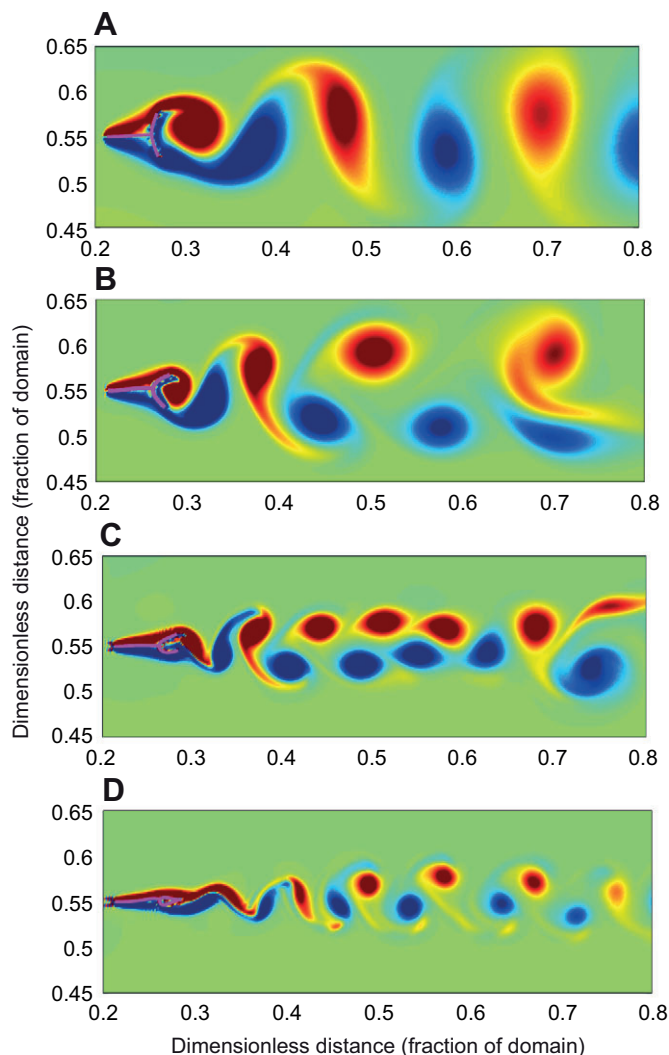
Physical models

When the flexible square cut-out is attached to a rigid rod, the sheet reconfigures into a stable U-shape. The wake consists of two oppositely spinning vortices (Fig. 10A). This was similar to what was reported for 2-D flows experimentally by Alben et al. (Alben et al., 2004) and through simulations in two dimensions by Zhu (Zhu, 2008) and in three dimensions by Zhu et al. (Zhu et al., 2011). The basic idea is that the low pressure region in the recirculation zone leads to reconfiguration of the beam (shape self-similarity) and a transition from the classical U^2 drag scaling of rigid bodies at high Re to a new $U^{4/3}$ drag law.

When the flexible square was attached to a flexible beam and immersed in a turbulent flow, significant oscillations occurred, and the sheet did not long retain the reconfigured U-shape. The time-averaged spatial distribution of velocity behind the sheet is shown in Fig. 10B. Notice that the recirculation zone was not as
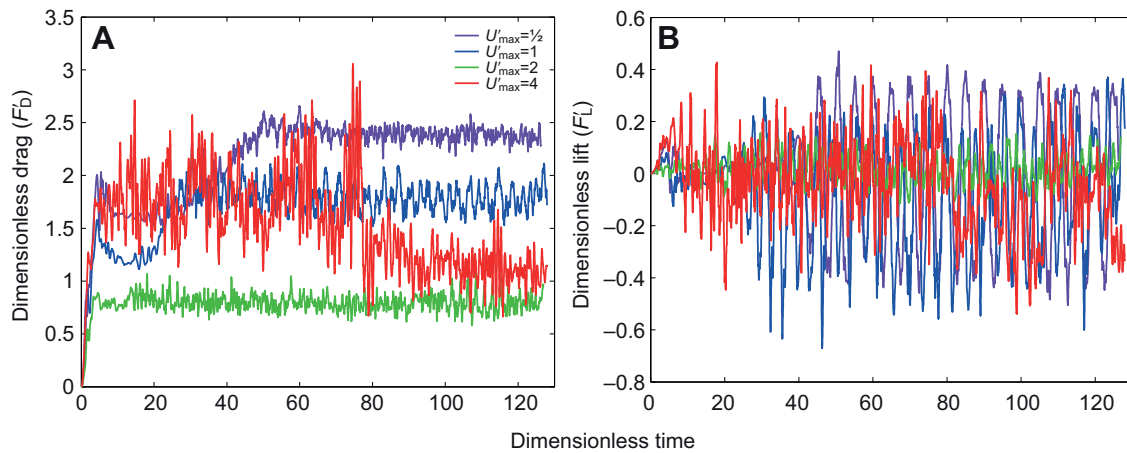
Fig. 9. Dimensionless lift and drag as functions of dimensionless time for four dimensionless velocities with $k'_{bend}=10^{-2}$. For free-stream velocities set to $U'_{max}=\frac{1}{2}$, 1, 2 and 4, the magnitudes of the dimensionless lift and drag decrease as the velocity increases because of the reconfiguration of the model leaf. Force coefficients then increase as the velocity increases to 4 as the interaction of the fluid and structure creates larger oscillations. Around $t'=80$, the tips of the model leaf adhere because of numerical effects, and the force coefficients as well as the oscillations decrease (see supplementary material Movie 5).

well formed as that shown for the case with the rigid attachment. The instantaneous distributions of velocity (Fig. 10C,D) showed periodic separation of regions of vorticity behind the sheet. The vortex shedding also induced forces acting perpendicular to the direction of flow. These observations were consistent with the behavior of aerial broad leaves when compared with flexible models attached to flexible beams, as described by Vogel (Vogel, 1989).

Wakes of herbaceous leaves and cones

To examine how actual broad leaves differ from the 2-D numerical simulations and physical models, PIV was used to resolve the wakes behind the leaves. As described by Vogel (Vogel, 2006), fully submerged *H. arifolia* and *V. papilionacea* leaves reconfigured into stable cones, even in the presence of highly turbulent flows. The cones became tighter as the flow speed was increased. Instantaneous snapshots of *V. papilionacea* leaves are
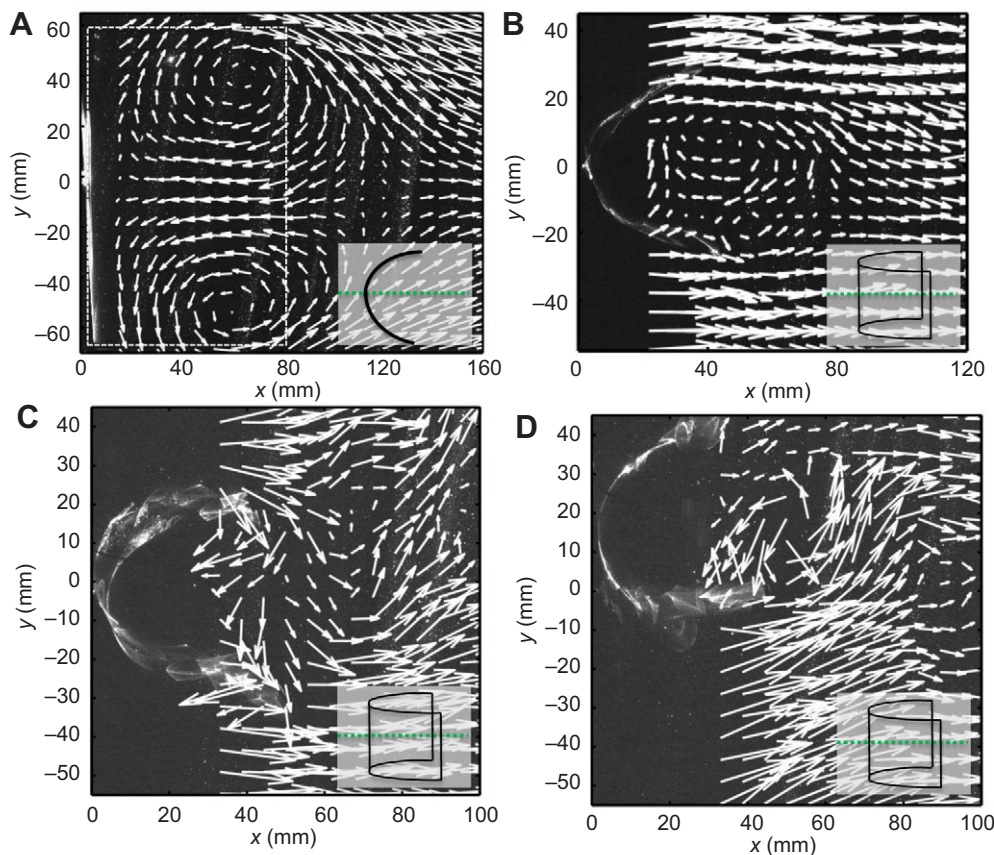

Fig. 10. Time-averaged velocity vectors obtained using PIV showing the wakes of a flexible sheet attached to a rigid beam (A) and a flexible sheet attached to a flexible beam (B) at $Re=80,000$. The insets show the laser plane as a green dotted line. Note that the laser plane would be coming towards the reader in the third dimension. The white dotted line in A shows the edges of the transparency that has reconfigured into a U-shape. Two stable oppositely spinning vortices are observed in A, which agrees with the results of Alben et al. (Alben et al., 2002). No structured wake is apparent in B. Instantaneous snapshots of the velocity fields in the wake of a flexible sheet attached to a flexible beam are shown in C and D. Strong shedding of vorticity and large oscillations are observed.
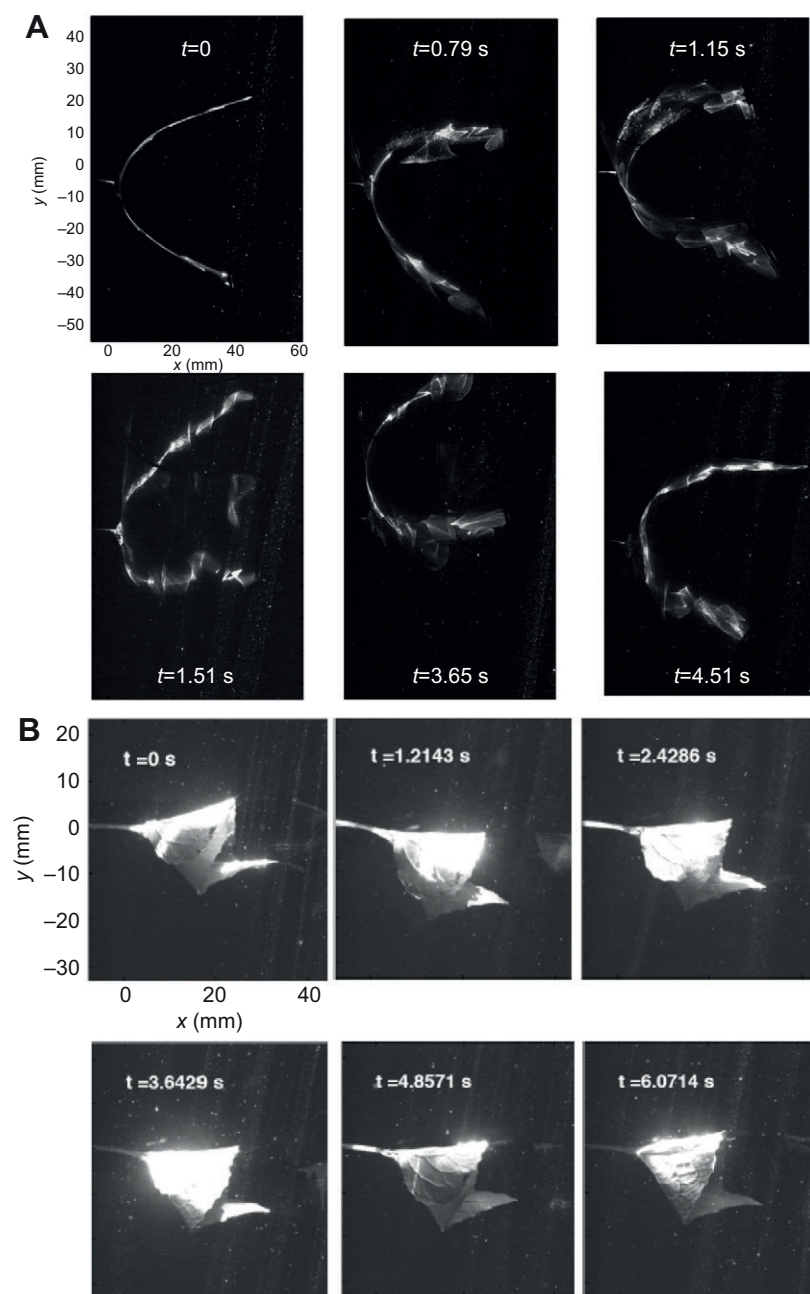
Fig. 11. Times series of images of a flexible sheet attached to a flexible wire (A) and a *Viola papilionacea* leaf (B) at *Re*=80,000. The flexible sheet reconfigures into a U-shape, but significant high-frequency distortions of the sheet are observed. Because of the turbulent nature of the fluid, the *V. papilionacea* leaf reconfigures into a cone shape with some movement.

compared with the flexible sheet models in Fig. 11. Large oscillations and high-frequency deformations of the flexible sheets were observed. Some motion of the *V. papilionacea* leaves was observed because of the strong unsteadiness of the flow, but the leaf retained its reconfigured shape throughout the experiment. Similar results were also observed for *H. arifolia*.

The time-averaged spatial distribution of velocity in the wake of *H. arifolia* is shown in Fig. 12A. A stable recirculation zone was formed in the wake of the reconfigured leaf, creating a low-pressure zone that aids in 'coning.' Significant shedding of vorticity was not observed for the ginger leaf, which reduced any hydrodynamic forces acting perpendicular to the flow. Similar behavior was also observed for the *V. papilionacea* leaves. These results were compared with time-averaged spatial distributions of the velocity in the wakes of sheets designed to reconfigure into cone shapes attached to flexible beams (Fig. 12B). A similar wake structure was observed. The

reconfiguration shape was also stable, although it appeared that the actual leaves were more stable.

Forces on flexible sheets and cones
To confirm that drag was reduced for flexible sheets that reconfigure into cones rather than U-shapes, forces on the transparency models were measured in the flow tank. The plan form (or projected, planar) area of both models was approximately $0.012\,m^2$ (see Tables 1 and 2 for details). No adjustment was made in the dimensionless force calculations to account for the reconfiguration of the leaves and models. The purpose of the physical models in this case was not so much to mimic the leaves but rather to compare these two reconfiguration shapes in general. The *H. arifolia* leaves, *V. papilionacea* leaves and physical models made out of transparency paper were almost neutrally buoyant, such that the effects of their additional masses relative to the fluid dynamic forces were
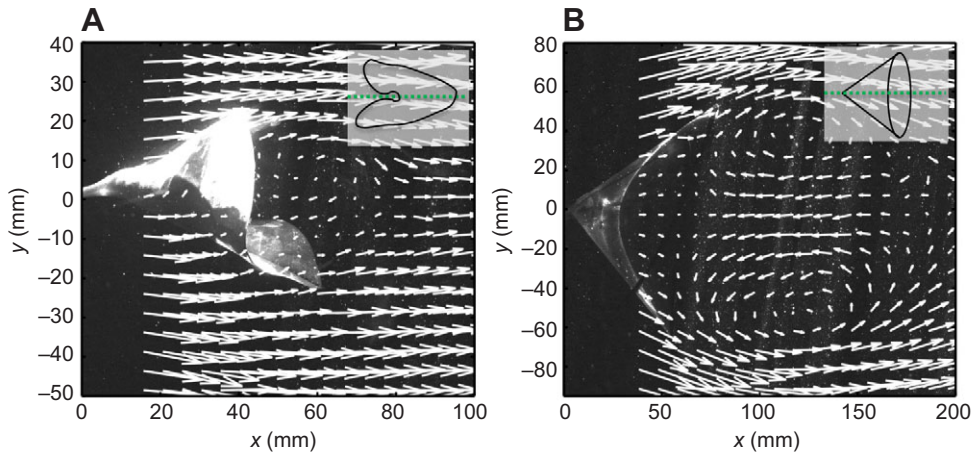
Fig. 12. Time-averaged velocity vectors obtained using PIV showing the stable recirculation zone in the wakes of an *H. arifolia* leaf (A) and a flexible sheet attached to a flexible beam that has reconfigured into a cone (B) at *Re*=80,000. The insets show the laser plane as a green dotted line. Note that the laser plane would be coming towards the reader in the third dimension. A pair of oppositely spinning vortices is apparent in the wake of the transparent sheet.

negligible. Fig. 13A shows the dimensionless drag averaged over 30 s *versus* free-stream velocity ranging from 0.3 to 1 m s⁻¹. The error bars show the standard deviations. For comparison, values for *Hexastylis* reported by Vogel (Vogel, 2006) are also plotted. In general, dimensionless drag decreases with velocity. Drag is lowest for *H. arifolia*, and the U-shape model generates the largest drag. Fig. 13B shows the peak dimensionless drag averaged over 1 s intervals for a total of 30 s. The error bars show the standard deviations. Peaks were taken over 1 s intervals because the dominant frequencies were on the order of 1–5 Hz. However, peaks taken over intervals of varying lengths show similar results. Peak drag is higher for the U-shape model than for the cone model and leaves for all velocities considered.

To consider the effects of the inertia of the leaves and models for the aerial case, both cone and U-shape transparency models were placed in a wind tunnel. Forces were also measured for *L. tulipifera* leaves for comparison. Mean dimensionless drag *versus* time for the two models and the *L. tulipifera* leaves for velocities ranging from 4 to 14 m s⁻¹ are shown in Fig. 14B. The error bars indicate the standard deviations. For velocities of 5 m s⁻¹ and greater, mean drag is generally lowest for the actual leaves and highest for the U-shape model. Large oscillations were observed for the U-shape model at velocities of 9 m s⁻¹ and greater, corresponding to the large standard deviations in drag. Fig. 14 shows the mean peak drag taken over 1 s intervals for the two physical models and the *L. tulipifera* leaves. The error bars show the standard deviations. The large peak dimensionless drag generated by the U-shape model is apparent for wind speeds greater than 9 m s⁻¹. Oscillations for the cone model and leaves were relatively small at these wind speeds, as indicated by the small standard deviations (see supplementary material Movies 6, 7). Forces were not measured for the U-shape model for velocities over 11 m s⁻¹ as violent oscillations caused the models to break.

Conclusions

The main result from the numerical simulation is that the addition of a flexible tether to the simple 2-D flexible beam model of a leaf results in larger oscillations, stronger vortex shedding and increased drag when compared with equivalent 2-D models with fixed attachments. The PIV results indicate that herbaceous broad leaves reconfigure into cones, and the wake behind the leaves contains a relatively stable pair of alternately spinning vortices. Physical models that reconfigure into cones exhibit similar behavior. Sheets that reconfigure into U-shapes (the 3-D analog of the simple 2-D beam model) exhibit strong oscillations and vortex shedding. Force

measurements on the physical models indicate that the large oscillations present in the U-shape models correspond to large peak drag forces. This effect is magnified in air when inertial effects of the models are non-negligible. These results confirm those reported
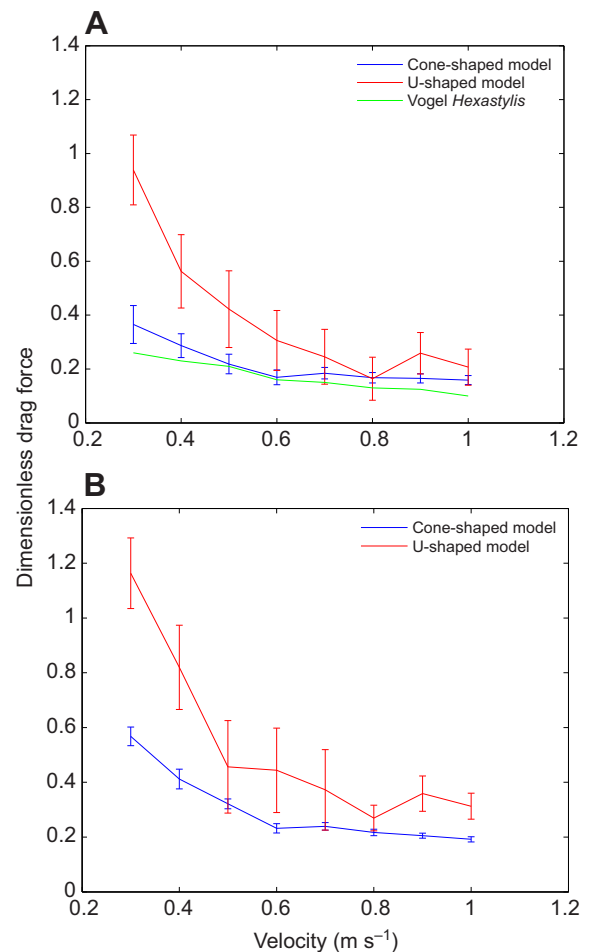

Fig. 13. (A) Mean dimensionless drag *versus* time for the cone and U-shape models with plan form areas of 0.012 m² in water for velocities ranging from 0.3 to 1 m s⁻¹. The green line denotes the drag measurements for *Hexastylis* leaves reported by Vogel (Vogel, 2006). Error bars denote the standard deviation of the forces measured over 30 s. (B) Mean peak dimensionless drag *versus* velocity for the cone and U-shape models. Mean peak forces were obtained over a 30 s interval by finding the peak force during each 1 s interval and taking the mean of those peaks.

Fig. 14. (A) Mean dimensionless drag *versus* time for the *L. tulipifera* leaves, the cone model and the U-shape model in air for velocities ranging from 4 to 14 m s^{-1}. Error bars denote the standard deviation of the forces measured over 30 s. (B) Mean peak dimensionless drag *versus* wind velocity for the *Liriodendron tulipifera* leaves, the cone model and the U-shape model. Mean peak forces were obtained over a 30 s interval by finding the peak force 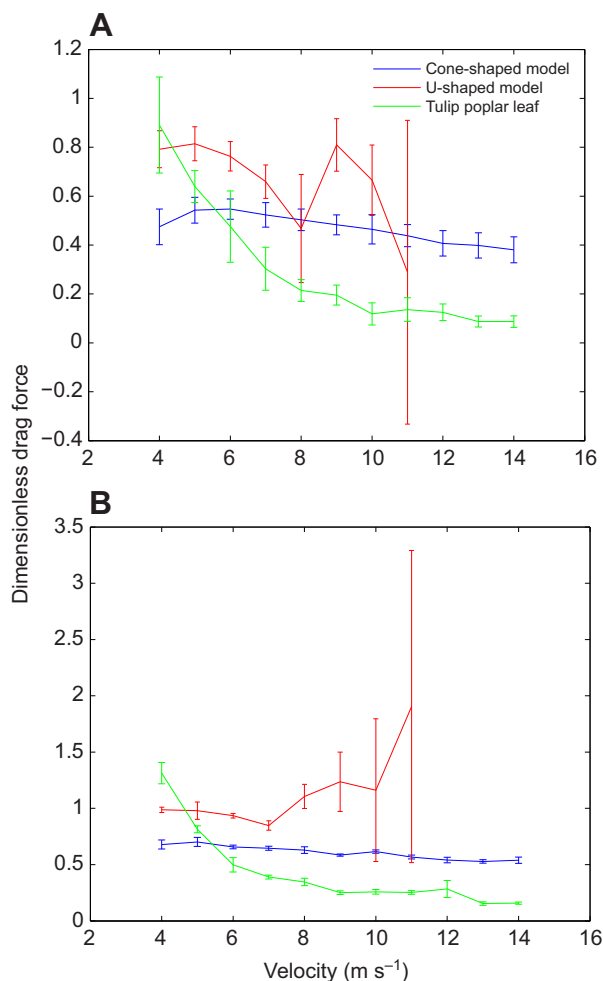during each 1 s interval and taking the mean of those peaks. Error bars denote the standard deviations. Peak drag is highest for the U-shape model, and the large jump in dimensionless force for this model corresponds to the onset of violent oscillations. Forces were not measured for the U-shape model for velocities over 9 m s^{-1} because these large oscillations caused the models to break

by Vogel (Vogel, 1989), which show that more than just flexibility is necessary for stable reconfiguration and drag reduction and suggest that the shape of the reconfiguration is important for drag reduction. This poses an interesting question for future work: are stable reconfiguration shapes advantageous to plants in terms of mechanical fitness? This study also complements a growing body of work using PIV to understand plant aerodynamics (e.g. Lentink et al., 2009; Marchetto et al., 2010).

Conical reconfiguration shapes are prevalent throughout the natural world (Vogel, 1994). A wide range of broad leaves reconfigure into cone shapes as both single leaves and clusters (Vogel, 1989; Vogel, 2006). The branches and fronds of flexible trees such as palms and willows appear to reconfigure into grouped conical shapes in strong winds and hurricanes. The daffodil *Narcissus* spp. (Etnier and Vogel, 2000) and sessile marine organisms such as sea anemones (Koehl,

1977a; Koehl, 1977b) reconfigure into cone shapes through deformations of the petals or tentacles, respectively. Macroalgae have adapted to wave-swept shores through increased flexibility and extensibility, which allows them to reconfigure (Vogel, 1984; Koehl, 1984; Koehl, 1986; Denny and Gaylord, 2002). Of course there are likely other strategies that may be used in place of or in addition to conical reconfigurations. For example, Gosselin and de Langre (Gosselin and de Langre, 2011) showed how plants such as pines may act as a poroelastic structures to reduce drag. There may also be situations in which flutter reduction is not desirable, such as for the purpose of enhanced canopy light through the fluttering of poplar leaves (Roden and Pearcy, 1993) or for the purpose of convective and evaporative heat transfer (Thom, 1968; Grant, 1983). In these cases, conical reconfiguration may not be present at wind speeds relevant to cooling and light transfer (0–4.5 m s^{-1}) when flutter could enhance these mechanisms.

Limitations and future work

This paper presents a first step towards understanding how the shape and material properties of broad leaves attached to flexible leafstalks can stabilize the leaf and presumably reduce the drag acting upon the plants. Although the numerical simulations and experiments are performed at different scales and dimensions and in different fluid media, each component of the study may be directly compared with previous work on the reconfiguration of flexible structures with rigid attachments. All of the results illustrate the important differences between modeling reconfiguration with flexible and fixed attachments.

Future work should quantify the dynamic properties of the forces acting on a variety of species of broad leaves over all biologically relevant flow speeds. It would also be worthwhile to thoroughly describe the 3-D structure of the wake behind the leaf in comparison to physical models over a range of speeds, in both steady and unsteady flows. Relatively simple physical models have been used to explore the role of shape and flexibility, but more realistic models would surely provide deeper insight into this problem. Finally, the applications of this work could also extend beyond gaining insight into the mechanical adaptations of plants in natural world. Understanding the mechanism of flutter reduction in broad leaves could inspire innovation in the engineering design of drag-reducing flexible structures such as sails, flags and cables.

REFERENCES
Alben, S. (2008). Optimal flexibility of a flapping appendage in an inviscid fluid. *J. Fluid Mech.* **614**, 355-380.
Alben, S. (2009). Simulating the dynamics of flexible bodies and vortex sheets. *J. Comput. Phys.* **228**, 2587-2603.
Alben, S., Shelley, M. and Zhang, J. (2002). Drag reduction through self-similar bending of a flexible body. *Nature* **420**, 479-481.
Alben, S., Shelley, M. and Zhang, J. (2004). How flexibility induces streamlining in a two-dimensional flow. *Phys. Fluids* **16**, 1694-1713.
Baker, C. J. (1995). The development of a theoretical model for the windthrow of plants. *J. Theor. Biol.* **175**, 355-372.
Blackburn, P., Petty, J. A. and Miller, K. F. (1988). An assessment of the static and dynamic factors involved in windthrow. *Forestry* **61**, 29-43.
Brüchert, F., Speck, O. and Spatz, H.-C. (2003). Oscillations of plants' stems and their damping: theory and experimentation. *Philos. Trans. R. Soc. B* **358**, 1487-1492.

de Langre, E. (2008). Effects of wind on plants. *Annu. Rev. Fluid Mech.* **40**, 141-168.

Denny, M. W. and Gaylord, B. (2002). The mechanics of wave-swept algae. *J. Exp. Biol.* **205**, 1355-1362.

Denny, M. W., Gaylord, B., Helmuth, B. and Daniel, T. (1998). The menace of momentum: dynamic forces on flexible organisms. *Limnol. Oceanogr.* **43**, 955-968.

Ennos, A. R. (1997). Wind as an ecological factor. *Trends Ecol. Evol.* **12**, 108-111.

Etnier, S. A. and Vogel, S. (2000). Reorientation of daffodil (*Narcissus: Amaryllidaceae*) flowers in wind: drag reduction and torsional flexibility. *Am. J. Bot.* **87**, 29-32.

Gosselin, F. P. and de Langre, E. (2011). Drag reduction by reconfiguration of a poroelastic system. *J. Fluids Struct.* **27**, 1111-1123.

Gosselin, F., de Langre, E. and Machado-Almeida, B. (2010). Drag reduction of flexible plates by reconfiguration. *J. Fluid Mech.* **650**, 319-342.

Grant, R. H. (1983). The scaling of flow in vegetative structures. *Boundary-Layer Meteorol.* **27**, 171-184.

Griffith, B. E., Luo, X., McQueen, D. M. and Peskin, C. S. (2009). Simulating the fluid dynamics of natural and prosthetic heart valves using the immersed boundary method. *Int. J. Appl. Mech.* **1**, 137-177.

Grünbaum, D., Eyre, D. and Fogelson, A. (1998). Functional geometry of ciliated tentacular arrays in active suspension feeders. *J. Exp. Biol.* **201**, 2575-2589.

Hamlet, C. H., Santhanakrishnan, A. and Miller, L. A. (2011). A numerical study of the effects of bell pulsation dynamics and oral arms on the exchange currents generated by the upside-down jellyfish *Cassiopea xamachana*. *J. Exp. Biol.* **214**, 1911-1921.

Kerzenmacher, T. and Gardiner, B. (1998). A mathematical model to describe the dynamic response of a spruce tree to the wind. *Trees* **12**, 385-394.

Koehl, M. A. R. (1977a). Effects of sea anemones on the flow forces they encounter. *J. Exp. Biol.* **69**, 87-105.

Koehl, M. A. R. (1977b). Mechanical diversity of the connective tissue of the body wall of sea anemones. *J. Exp. Biol.* **69**, 107-125.

Koehl, M. A. R. (1984). How do benthic organisms withstand moving water? *Am. Zool.* **24**, 57-70.

Koehl, M. A. R. (1986). Seaweeds in moving water: form and mechanical function. In *On the Economy of Plant Form and Function* (ed. T. J. Givnish), pp. 603-634. Cambridge: Cambridge University Press.

Lentink, D., Dickson, W. B., van Leeuwen, J. L. and Dickinson, M. H. (2009). Leading-edge vortices elevate lift of autorotating plant seeds. *Science* **324**, 1438-1440.

Luongo, A. and Piccardo, G. (1998). Non-linear galloping of sagged cables in 1:2 internal resonance. *J. Sound Vibrat.* **214**, 915-940.

Marchetto, K. M., Williams, M. B., Jongejans, E., Auhl, R. and Shea, K. (2010). Applications of particle image velocimetry for seed release studies. *Ecology* **91**, 2485-2492.

Miller, L. A. (2005). Structural dynamics and resonance in plants with nonlinear stiffness. *J. Theor. Biol.* **234**, 511-524.

Niklas, K. J. (1992a). Petiole mechanics, light interception by lamina, and economy in design. *Oecologia* **90**, 518-526.

Niklas, K. J. (1992b). *Plant Biomechanics: An Engineering Approach to Plant Form and Function*. Chicago: University of Chicago Press.

Niklas, K. J. (1999). A mechanical perspective on foliage leaf form and function. *New Phytol.* **143**, 19-31.

Peskin, C. S. and McQueen, D. M. (1996). Fluid dynamics of the heart and its valves. In *Case Studies in Mathematical Modeling: Ecology, Physiology, and Cell Biology*, 2nd edn (ed. H. G. Othmer, F. R. Adler, M. A. Lewis and J. C. Dallon), pp. 309-338. New Jersey: Prentice-Hall.

Peskin, C. S. and Printz, B. F. (1993). Improved volume conservation in the computation of flows with immersed elastic boundaries. *J. Comput. Phys.* **105**, 33-46.

Roden, J. S. and Pearcy, R. W. (1993). Effect of leaf flutter on the light environment of poplars. *Oecologia* **93**, 201-207.

Schouveiler, L. and Boudaoud, A. (2006). The rolling up of sheets in a steady flow. *J. Fluid Mech.* **563**, 71-80.

Speck, T. and Burgert, I. (2011). Plant stems: Functional design and mechanics. *Annu. Rev. Mater. Res.* **41**, 169-193.

Steinberg, V. (2002). Hydrodynamics: bend and survive. *Nature* **420**, 473.

Theckes, B., de Langre, E. and Boutillon, X. (2011). Damping by branching: a bioinspiration from trees. *Bioinspir. Biomim.* **6**, 046010.

Thom, A. S. (1968). The exchange of momentum, mass, and heat between an artificial leaf and the airflow in a wind tunnel. *Q. J. R. Meteorol. Soc.* **94**, 44-55.

Tomita, S., Kawase, M., Shinohara, H. and Fuchigami, T. (1988). Suppression of galloping oscillation for a self-supporting opticalfiber cable. *J. Lightwave Technol.* **6**, 186-190.

Tucker, V. A. and Parrott, G. C. (1970). Aerodynamics of gliding flight in a falcon and other birds. *J. Exp. Biol.* **52**, 345-367.

Tytell, E. D., Hsu, C.-Y., Williams, T. L., Cohen, A. H. and Fauci, L. J. (2010). Interactions between internal forces, body stiffness, and fluid environment in a neuromechanical model of lamprey swimming. *Proc. Natl. Acad. Sci. USA* **107**, 19832-19837.

Vincent, J. F. V. (1990). Fracture properties of plants. *Adv. Bot. Res.* **17**, 235-287.

Vogel, S. (1984). Drag and flexibility in sessile organisms. *Am. Zool.* **24**, 37-44.

Vogel, S. (1989). Drag and reconfiguration of broad leaves in high winds. *J. Exp. Bot.* **40**, 941-948.

Vogel, S. (1994). *Life in Moving Fluids: The Physical Biology of Flow*, 2nd edn. Princeton, NJ: Princeton University Press.

Vogel, S. (2006). Drag reduction by leaf aquaplaning in *Hexastylis* (Aristolochiaceae) and other plant species in floods. *J. N. Am. Benthol. Soc.* **25**, 2-8.

Vogel, S. and LaBarbera, M. (1978). Simple flow tanks for research and teaching. *Bioscience* **28**, 638-643.

Wilson, J. (1984). *Dynamics of offshore structures*, 2nd edn. New York: John Wiley and Sons.

Zhu, L. (2007). Viscous flow past a flexible fibre tethered at its centre point: vortex shedding. *J. Fluid Mech.* **587**, 217-234.

Zhu, L. (2008). Scaling laws for drag of a compliant body in an incompressible viscous flow. *J. Fluid Mech.* **607**, 387-400.

Zhu, L., He, G., Wang, S., Miller, L., Zhang, X., You, Q. and Fang, S. (2011). An immersed boundary method based on the lattice Boltzmann approach in three dimensions, with application. *Comput. Math. Appl.* **61**, 3506-3518.